Chinese Physics Letters

LETTER

Ultrafast Proton and Charge Transfer in the Coulomb Explosion of HCl Dimer

Cite as: Xinning Zhao *et al*. 2026 *Chin. Phys. Lett.* **43** 070301

DOI CSTR

Recommended Articles

Direct Observation on H-Elimination Enhancement from C_2H_4 through Non-Adiabatic Process by Femtosecond Laser Induced Coulomb Explosion

Wuwei Jin, Chuncheng Wang, Xiaoge Zhao, Yizhang Yang, Dianxiang Ren, Zejin Liu, Xiaokai Li, Sizuo Luo, and Dajun Ding

Chin. Phys. Lett. **41**, (2024)

Charge Transfer at the $Ni_3InN/SrVO_3$ Heterointerfaces

Ting Cui *et al*.

Chin. Phys. Lett. **42**, 100705 (2025)

Superexchanges and Charge Transfer in $La_3Ni_2O_7$ Thin Films

Yuxun Zhong, Wéi Wú, and Dao-Xin Yao

Chin. Phys. Lett. **43**, 030713 (2026)

Ultrafast Carrier Dynamics in $Ba_6Cr_2S_{10}$ Modified by Toroidal Magnetic Phase Transition

Litong Jiang *et al*.

Chin. Phys. Lett. **41**, (2024)

Photodoping-Modified Charge Density Wave Phase Transition in WS_2/1T-TaS_2 Heterostructure

Rui Wang, Jianwei Ding, Fei Sun, Jimin Zhao, and Xiaohui Qiu

Chin. Phys. Lett. **41**, (2024)

Revealing Light-Induced Charge Density Wave Melting and Carrier Redistribution in 1T-$TiSe_2$

Wanying Chen, Haoyuan Zhong, Changhua Bao, Fei Wang, Xuanxi Cai, Chenxia Yun, Hao Teng, Zhiyi Wei, and Shuyun Zhou

Chin. Phys. Lett. **42**, 017101 (2025)

A series journal of Chinese Physical Society distributed by IOP Publishing

Chinese Physics Letters

Chin. Phys. Lett. **43** 070301 (2026)

LETTER

DOI: 10.1088/0256-307X/43/7/070301
CSTR: 32039.14.0256-307X.43.7.070301

Ultrafast Proton and Charge Transfer in the Coulomb Explosion of HCl Dimer

Xinning Zhao(赵欣宁)[1,†], Ting Xu(许婷)[2,†], Di Ren(任迪)[1], Zhiyuan Liu(刘志远)[1], Xiaokai Li(李孝开)[3,4], Chuncheng Wang(王春成)[3,4], Yong Wu(吴勇)[5], Xiaoqing Hu(胡晓青)[5,*], Sizuo Luo(罗嗣佐)[3,4,*], and Dajun Ding(丁大军)[3,4,*]

[1]College of Materials Science and Engineering, Changchun University of Technology, Changchun 130012, China
[2]College of Science, Xi'an University of Science and Technology, Xi'an 710054, China
[3]Institute of Atomic and Molecular Physics, Jilin University, Changchun 130012, China
[4]Jilin Provincial Key Laboratory of Transient Quantum Process Control and Application, Jilin University, Changchun 130012, China
[5]Key Laboratory of Computational Physics, Institute of Applied Physics and Computational Mathematics, Beijing 100088, China

[†]These authors contributed equally to this work.
[*]Corresponding authors. Email: xiaoqing-hu@foxmail.com; luosz@jlu.edu.cn; dajund@jlu.edu.cn

The ultrafast dissociation of hydrogen-bonded clusters offers a fundamental route to studying energy relaxation and intermolecular proton transfer. Here, we investigate the three-body fragmentation of the HCl dimer following strong-field ionization into tricationic states. Angle-resolved kinetic energy measurements reveal distinct breakup mechanisms: a direct Coulomb explosion and the two pathways mediated by intermolecular charge transfer and proton transfer. The kinetic energy distributions of the Cl^+ and HCl^+ fragments evolve from a single peak to a double-peak structure as the relative emission angle increases. Ab initio calculations of the tricationic potential energy surface indicate that this splitting arises from competing charge-transfer and proton-transfer driven dissociation pathways. These results illustrate how ultrafast charge redistribution and proton motion govern the strong-field dissociation dynamics of a prototypical hydrogen-bonded cluster.

The interaction of strong ultrafast lasers with matter gives rise to a variety of fundamental processes, including high-order harmonic generation [1,2], photoionization [3–5], molecular dissociation, and Coulomb explosion [6–14]. These processes provide deep insights of ultrafast structural and electronic dynamics in atoms, molecules, and clusters. In particular, proton motion in hydrogen-containing systems plays a central role in many physical, chemical, and biological processes, ranging from molecular rearrangement and reaction product formation to DNA damage and photosynthetic reactions [15–22]. Owing to its small mass and pronounced quantum nature, the proton exhibits extremely rapid dynamics such as roaming, transfer, and hopping, which often occur on femtosecond time scales and remain challenging to observe directly [23–25]. Recent studies have shown that strong-field ionization can initiate proton migration within tens of femtoseconds, during which the proton explores complex potential-energy surfaces and facilitates the formation of new reaction products. In addition, proton roaming has been identified as a key pathway leading to the formation of molecular ions such as H_2^+ and H_3^+ following strong-field or collision-induced fragmentation [20,23,26–29].

In molecular clusters, intermolecular hydrogen bonding introduces additional pathways for proton transfer that are absent in isolated molecules. Such intermolecular motion can trigger ultrafast charge redistribution, structural rearrangement, and the formation of new ionic species. For example, femtosecond time-resolved ion spectroscopy of D_2 dimers has revealed the ultrafast formation of D_3^+ following strong-field ionization [30–32]. Similar mechanisms have been predicted and observed in small molecular reactions such as H_2 + CO, where ultrafast formation of C-H bonds leads to transient HCO products [33]. These studies highlight the key role of intermolecular proton motion in hydrogen-bond reorganization and energy redistribution in complex systems. Complementary ultrafast probes have further advanced the study of proton transfer in hydrogen-bonded networks. Time-resolved soft-x-ray spectroscopy [24], ultrafast electron diffraction [25], and two-dimensional infrared spectroscopy [34] have enabled real-time tracking of proton dynamics in water, revealing the formation of transient $OH(H_3O^+)$ radical cations within ~140 fs and vibrational motion in Zundel-type hydration structures [35]. Despite these advances, direct observation of correlated charge and proton transfer during cluster fragmentation remains limited. Hydrogen-bonded clusters such as HCl dimers, NH_3 dimers, formic acid dimers, and hydrated biomolecules have therefore attracted considerable interest in both ultrafast laser and collision experiments [20,36–42]. Proton motion in these systems represents one of the fastest nuclear processes in femtochemistry and may also contribute to the high biological effectiveness of heavy-ion irradiation [22,43,44]. experimental techniques must be capable of resolving transient molecular structures while effectively suppressing background signals. Coulomb explosion imaging (CEI) offers a powerful solution by reconstructing molecular geometry from the momenta of fragment ions generated during Coulomb-dominated breakup [6–12]. This approach has enabled visualization of molecular and cluster structures, as well as the observation of proton roaming and transfer during ultrafast fragmentation [45–49].

In this work, we investigate the three-body fragmentation dynamics of the HCl dimer induced by strong femtosecond laser pulses. Using coincidence momentum imaging, we measure the correlated momenta of the breakup channel, $(HCl)_2^{3+} \rightarrow H^+ + Cl^+ + HCl^+$. Angle-energy correlation analysis reveals two distinct mechanisms: direct Coulomb explosion, and fragmentation mediated by ultrafast charge and proton transfer. Combined with high-level potential-energy-surface calculations, the results provide direct insight into the role of intermolecular charge redistribution and proton motion in the ultrafast dissociation of hydrogen-bonded molecular clusters.

The experiment was performed using a COLTRIMS (cold target recoil ion momentum spectroscopy) apparatus [50,51], as shown in Fig. 1(a). Details of the setup have been described elsewhere [40,41,52]. A supersonic molecular beam was generated by expanding a 1:1 mixture of HCl and Ar at a backing pressure of 0.7 bar

Received 24 March 2026; accepted 6 June 2026; published 15 July 2026
© 2026 Chinese Physical Society and IOP Publishing Ltd. All rights, including for text and data mining, AI training, and similar technologies, are reserved.

Check for updates

through a 30 μm nozzle, producing HCl dimers with an estimated abundance of ~1% in the beam. The molecular beam was interacted by linearly polarized femtosecond laser pulses (800 nm, 35 fs, 1 kHz) with a peak intensity of 8×10^{14} W/cm^2. Fragment ions produced by strong-field ionization and subsequent Coulomb explosion were guided by a uniform electric field (~16.8 V/cm) toward time- and position-sensitive detectors, allowing full three-dimensional momentum reconstruction. To ensure reliable coincidence detection, the count rate was maintained below 0.4 events per laser shot. Momentum conservation conditions were applied during offline analysis to suppress false coincidence [53]. To elucidate the dissociation dynamics of $(HCl)_2^{3+}$, potential energy curves and surfaces were calculated using *ab initio* electronic structure methods. The neutral structure of the HCl dimer [54,55], characterized by bending angles of 90° and 171°, with an intermolecular distance $R = 2.27$ Å and intramolecular distance $r = 1.28$ Å, is shown in the inset of Fig. 1(a). Initial calculations were performed at the Hartree–Fock level, followed by configuration interaction (CI) and complete active space self-consistent field (CASSCF) calculations [56,57]. To achieve quantitative agreement with the experimental observations, multi-reference configuration interaction (MRCI) calculations were subsequently performed, enabling accurate reconstruction of the potential energy surfaces governing the dissociation pathways of the HCl dimer.

Three-body fragmentation events were identified using photoion-photoion coincidence (PIPICO) measurements. The extracted PIPICO correlation between the time-of-flight (TOF) of Cl^+ and the summed TOF of the H^+ and HCl^+ fragments is shown in Fig. 1(b). Due to momentum conservation, the momentum sum of all three fragments is close to zero, with a narrow distribution determined mainly by the initial momentum of HCl_2 and the recoil momentum during the strong field ionization. As the TOF of an ion depends on its momentum and mass, the three-body Coulomb explosion channel leads to a sharp diagonal line in the PIPICO map [40,43,58]. Three sharp lines are observed, arising from contributions of the two chlorine isotopes, ^{35}Cl (75.77%) and ^{37}Cl (24.23%). The corresponding dissociation channels are

$$\text{Channel 1}: \left(H_2{}^{35}Cl_2\right)^{3+} \longrightarrow H^+ + {}^{35}Cl^+ + H^{35}Cl^+$$

$$\text{Channel 2}: \left(H_2{}^{37}Cl_2\right)^{3+} \longrightarrow H^+ + {}^{37}Cl^+ + H^{37}Cl^+$$

$$\text{Channel 3}: \left(H_2{}^{35}Cl{}^{37}Cl\right)^{3+} \longrightarrow H^+ + {}^{35}Cl^+ + H^{37}Cl^+$$

$$\text{Channel 4}: \left(H_2{}^{35}Cl{}^{37}Cl\right)^{3+} \longrightarrow H^+ + {}^{37}Cl^+ + H^{35}Cl^+$$

No significant differences are observed among these isotopic channels in either the kinetic energy release or the momentum correlation patterns discussed below. Because the kinetic energy distributions are primarily determined by the underlying potential energy surfaces and are therefore largely insensitive to isotopic substitution, all isotopic contributions are combined in the kinetic-energy analysis to improve statistical accuracy.

The black solid line in Fig. 1(c) shows the kinetic energy release (KER) spectra for the three-body fragmentation of the triply charged HCl dimer. For comparison, the figure also includes the KER distribution for the two-body Coulomb explosion of HCl monomers ($HCl^{2+} \rightarrow H^+ + Cl^+$, blue curve) and the summed kinetic energy of the H^+ and Cl^+ fragments from the dimer three-body breakup (red dash curve). The KER accumulated from the dissociation of dimer is significantly larger than that of the monomer channel. For the direct fragmentation of HCl^{2+}, the KER spectrum exhibits three peaks at 5.7, 6.3, and 8.2 eV, in agreement with previous measurements [59], those three peaks are attributed to dissociation from the $^3\Sigma$, $^1\Delta$, and $^1\Sigma$ states of HCl^{2+}, respectively [60]. In contrast, the KER acquired from the three-body breakup of the tricationic dimer peaks near 12 eV (black curve). A weaker contribution around 8 eV can be assigned to monomer-like dissociation channels embedded in the cluster environment. The overall shift toward higher KER indicates that the presence of the neighboring HCl^+ ion strongly modifies the Coulomb explosion dynamics. In additional, the observed three-peaks KER distribution from monomer merge into a broad asymmetry profile due to the the neighboring HCl^+ ion modifies the potential energy surface and redistribute the kinetic energy between fragments during three-body fragmentation process.

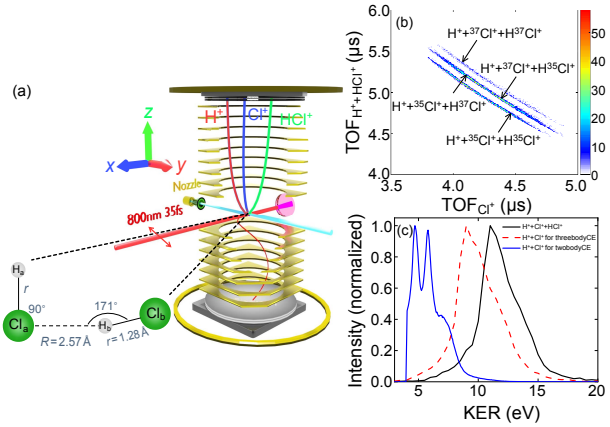

Fig. 1. (a) Schematic of the experimental setup. The neutral structure of the HCl dimer is indicated by the dashed lines, with bending angles of 90° and 171°, and an intermolecular distance $R = 2.57$ Å and intra-distance $r = 1.28$ Å [54,55]. (b) PIPICO spectrum of $(HCl)_2^{3+}$ three-body fragmentation, derived from the correlation between the TOF of Cl^+ and the summed TOF of H^+ and HCl^+. The three coincidence lines arise from the two chlorine isotopes, ^{35}Cl and ^{37}Cl. (c) Kinetic energy release (KER) distributions for dimer fragmentation: total KER (black solid line), summed kinetic energy for H^+ and Cl^+ fragments from dimer (red dashed line), and KER for Coulomb explosion of HCl monomers (blue solid line).

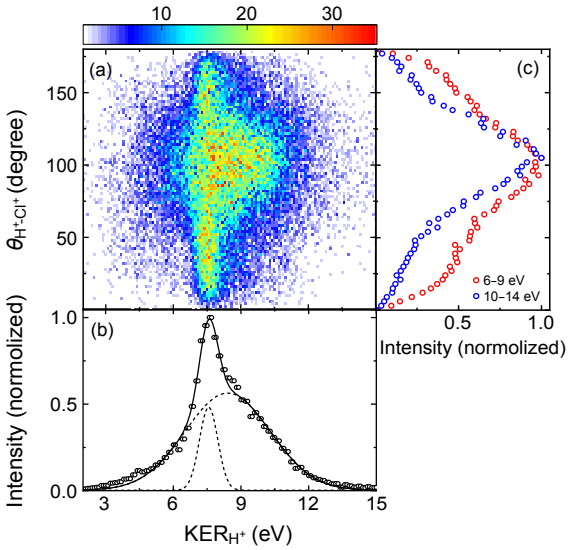

Fig. 2. (a) Correlation map between the experimentally measured kinetic energy release (KER) of H^+ and the scattering angle between H^+ and Cl^+. (b) KER spectrum of H^+ fragments with double Gaussian fitting. (c) Angular distributions of H^+ fragments obtained by integrating KER within 6–9 eV and 10–14 eV energy ranges.

We further analyze the correlation between the proton kinetic energy and the emission angle between H^+ and Cl^+ momenta, $\theta_{H^+\text{-}Cl^+}$, as shown in Fig. 2(a), to characterize its fragmentation mechanism. Two distinct features are observed. The first exhibits a broad angular distribution extending from 0° to 180° with a narrow kinetic-energy peak around 7.5 eV, indicating nearly isotropic proton emission. The second feature shows a pronounced angular maximum near 105° accompanied by a broader kinetic-energy distribution extending from approximately 3 to 12 eV and peaking near 9 eV. The corresponding KER and angular distributions are summarized in Figs. 2(b) and 2(c).

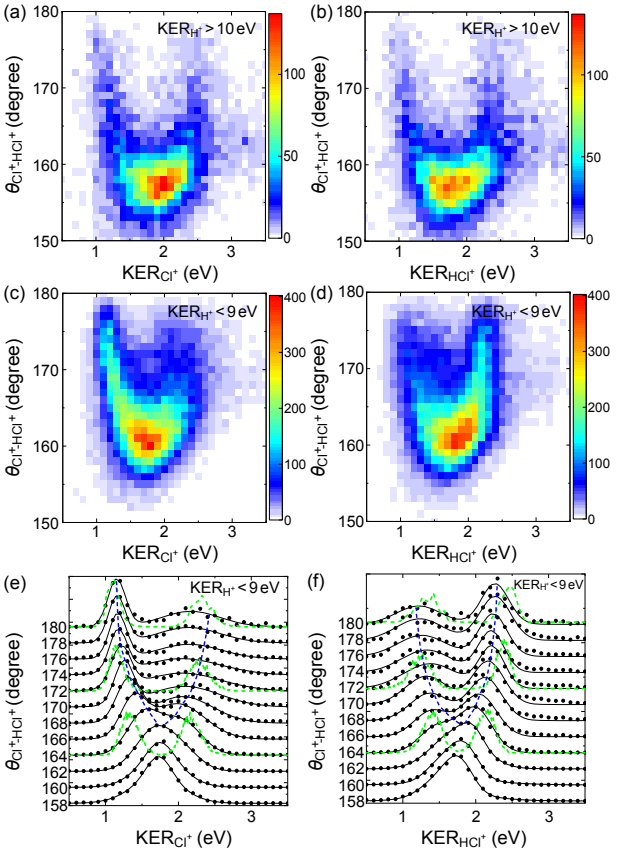

Fig. 3. (a) and (b) show the experimentally measured correlation between the kinetic energy release of Cl^+/HCl^+ fragments and the scattering angle ($\theta_{Cl^+\text{-}HCl^+}$) for events where H^+ energy is larger than 10 eV. (c) and (d) display the corresponding results for H^+ energies is smaller than 9 eV. (e) and (f) illustrate the angular-dependent KER intensity distributions for Cl^+ and HCl^+, respectively. The black solid lines represent maximum-normalized profiles derived from (c) and (d), with coordinate shifting applied to enhance visualization, and the blue dashed lines indicate the angular dependence of the KER peak evolution. The green dashed lines are calculated KER distributions at corresponding angles.

To distinguish these mechanisms, the data are further separated according to the distribution of proton's kinetic energy as seen in Figs. 2(a) and 2(b). Events with $KER_{H^+} < 9$ eV and $KER_{H^+} > 10$ eV are analyzed separately. The resulting correlations between the kinetic energies of Cl^+ and HCl^+ and their relative emission angle $\theta_{Cl^+\text{-}HCl^+}$ are shown in Fig. 3. For high-energy protons shown in Figs. 3(a) and 3(b), the relative emission angle is narrowly confined around 157°, characteristic of a direct Coulomb explosion from the equilibrium dimer geometry [8,41]. In this case, the outer proton (H_a^+) is emitted promptly after the formation of the tricationic state, followed by Coulomb repulsion between Cl_a^+ and $H_b Cl_b^+$. In the case of low-energy protons presented in Figs. 3(c) and 3(d), the kinetic energies of Cl^+ and HCl^+ vary strongly as the emission angle approaches 180°, indicating a broad distribution of fragmentation geometries and delayed proton emission. Further insight is obtained from the emission-angle-dependent kinetic-energy distributions of the Cl^+ and HCl^+ fragments shown in Figs. 3(e) and 3(f). At $\theta_{Cl^+\text{-}HCl^+} \approx 158°$, both fragments exhibit single-peaked kinetic-energy distributions centered near 1.6–1.7 eV. However, as the emission angle approaches 180°, the spectra evolve into a pronounced double-peak structure. For Cl^+, the peaks appear near 1.2 and 2.3 eV, while the HCl^+ distribution shows complementary intensity variations, indicating a redistribution of energy between the two fragments. This spectral splitting occurs when Cl^+ and HCl^+ recoil in opposite directions, corresponding to $\theta_{Cl^+\text{-}HCl^+} \approx 180°$, where the proton is emitted either parallel or antiparallel to the Cl^+ momentum.

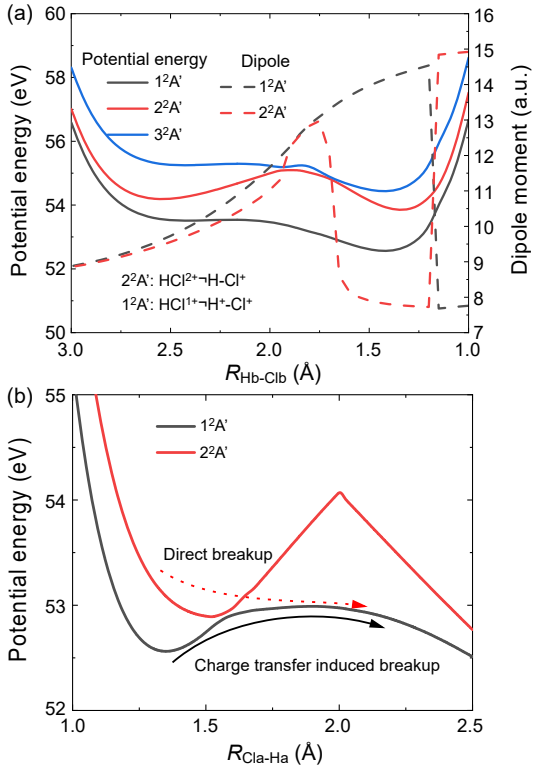

Fig. 4. (a) The potential energy curves of $1^2A'$, $2^2A'$, and $3^2A'$ states of the $(HCl)_2^{3+}$ when elongation the bond of H_b and Cl_b, calculated using the MRCI method. The corresponding dipole moments of $1^2A'$, $2^2A'$ are calculated and shown with the dashed curves. (b) The calculated potential curves of $1^2A'$, $2^2A'$ when stretching the distance between H_a and Cl_a, the direct and charge transfer induced breakup pathways are illustrated.

To elucidate the underlying mechanism, we performed ab initio calculations of the potential energy curves for the lowest electronic states of $(HCl)_2^{3+}$ at the MRCI/cc-pVTZ level using the MOLPRO package. In our calculations, the active space includes all orbitals of Cl ($n = 3$ and $n = 4$) and H ($n = 1$). We imposed a restriction that a maximum of two electrons occupy the $n = 4$ orbitals. This choice ensures a balanced description of the relevant electronic configurations while maintaining computational feasibility. We neglected the effect of spin–orbit coupling on the potential energy curves, because the energy difference it introduces is much smaller than the energy released in the Coulomb explosion. The potential energy curves calculated along the Cl_b-H_b coordinate are shown in Fig. 4(a). Analysis of the dipole moments indicates that the ground state corresponds to the charge-localized configuration $H_a Cl_a^+$-$H_b Cl_b^{2+}$, whereas the first excited state corresponds to $H_a Cl_a^{2+}$-$H_b Cl_b^+$. In the excited state, the hydrogen atom located between the two chlorine atoms carries a positive charge, whereas the outer hydrogen remains largely neutral. This charge localization enhances Coulomb repulsion among the fragments and promotes rapid dissociation. As the outer H_a-Cl_a bond stretches, the $1^2A'$ and $2^2A'$ potential curves intersect as seen in Fig. 4(b), forming a conical intersection that enables efficient nonadiabatic charge transfer between the two HCl molecules. In the excited states of $H_a Cl_a^{2+}$-$H_b Cl_b^+$, the unstable dicationic state rapidly dissociates, leading to direct Coulomb explosion. This channel exhibits the narrow angular distribution of $\theta_{H^+\text{-}Cl^+}$, as shown in Fig. 2(a). during strong-field ionization that populates the trication, the H–Cl bond can stretch as early as the mono- or dicationic stage, giving rise to an exceptionally broad KER distribution (~3–12 eV) upon tricationic dissociation. In contrast, on the surface of the ground-state, the $H_a Cl_a^+$ remains bound, and fragmentation occurs after charge transfer through the conical intersection. Before dissociation occurs, the bond angle $\angle H_a$-Cl_a-H_b rotates toward larger angles under the influence of

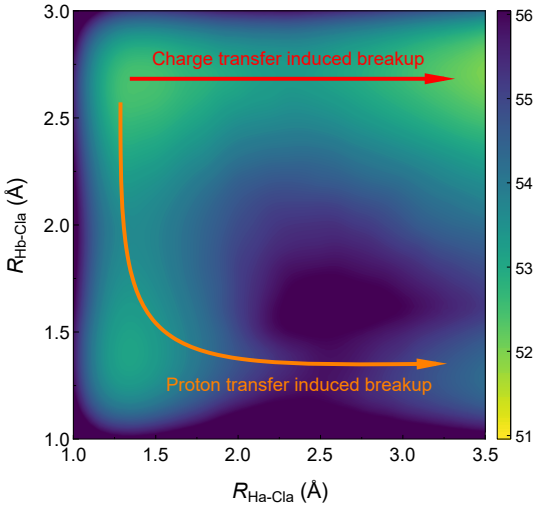

Fig. 5. The potential energy surface of the $(HCl)_2^{3+}$ when stretching the distances between two proton H_a and H_b with Cl_a, calculated using the MRCI method. Two dissociation pathways induced by charge transfer and proton transfer are marked with the red arrow and blue curve arrow.

the Coulomb potential. In this channel, the kinetic energy of the produced protons is tightly limited by the potential well depth and the crossing point energy, thus only cover over a small range. This matches the region in Fig. 2(a), which shows a broad angular distribution yet a narrow kinetic energy distribution.

The calculated two-dimensional potential energy surfaces are presented in Fig. 5, where two distinct dissociation channels can be identified. Although in both pathways the proton that appears in the final dissociation products originates from H_a, its dissociation dynamics differ significantly. One channel involves charge-transfer-induced fragmentation dynamics. Following charge transfer, the ionic system can be described as H_a^+-Cl_a^+-$H_b\,Cl_b^+$, with Cl_a^+ occupying a central position and $H_b\,Cl_b^+$ located at the periphery. In this configuration, Coulomb repulsion among the three bodies imparts a higher kinetic energy to $H_b\,Cl_b^+$ compared to Cl_a^+. In contrast, the proton transfer mechanism leads to a precursor geometry of H_a^+-$Cl_a\,H_b^+$-Cl_b^+, where $Cl_a\,H_b^+$ resides in the intermediate region and Cl_b^+ is situated at the terminal end. Consequently, the kinetic energy of Cl_b^+ exceeds that of $Cl_a\,H_b^+$ in this pathway. Moreover, as shown in the figure, the charge-transfer channel has a lower energy barrier, making it the dominant contributor to the three-body dissociation process—consistent with experimental observations. Ultimately, the three-body fragmentation arising from these two distinct mechanisms gives rise to the bimodal structure observed in the experiment.

In the absence of electronic coupling, the charge-transfer pathway exhibits a barrier of about 3.6 eV, however, the conical intersection between the $1^2A'$ and $2^2A'$ states reduces this barrier to approximately 0.4 eV, strongly enhancing the probability of charge redistribution. These competing charge-transfer and proton-transfer mechanisms naturally explain the experimentally observed kinetic-energy splitting of the Cl^+ and HCl^+ fragments under larger emission angles. Since proton emission can occur either parallel or antiparallel to the Cl^+ momentum, momentum conservation leads to different energy partitioning between the chlorine-containing fragments. We have performed semiclassical dynamics simulations of H_a^+-$Cl_a\,H_b^+$-Cl_b^+ and H_a^+-Cl_a^+-$H_b\,Cl_b^+$ based on the Coulomb potential approximation and *ab initio* calculations. Here, the interactions between H_a and the remaining fragments ($Cl_a\,H_b^+$-Cl_b^+ or Cl_a^+-$H_b\,Cl_b^+$) are obtained from *ab initio* calculations. In contrast, the interaction between HCl^+ and Cl^+ is described by an approximated Coulomb potential. The initial configuration of the simulation is assumed to be the structure after charge transfer or proton transfer has occurred. The initial bond angles of H-HCl-Cl and H-Cl-HCl were scanned from 90° to 180°. The calculated kinetic energies of Cl^+ and HCl^+ fragments are compared with experimental results. The corresponding simulated kinetic energy distributions at specific angles are shown with the green dashed lines in Figs. 3(e) and 3(f). The results reveal that the experimentally observed double-peak structure at $\theta \approx 180°$ originates from the fragmentation of near-linear molecular configurations when emitted under parallel or anti-parallel directions, as we explained above. Moreover, the observation that the combined kinetic energy of Cl^+ and HCl^+ follows a Coulomb potential corresponding to two singly charged ions further indicates that proton motion precedes the major Coulomb-driven separation of the heavy fragments. Together, the experimental and theoretical results demonstrate that fragments with a narrow relative angular distribution arise from direct Coulomb explosion, whereas the signal with broad relative angular distributions corresponds to ultrafast intermolecular charge transfer and proton transfer occurring prior to the Coulomb explosion.

In summary, we have investigated the ultrafast three-body dissociation of the HCl dimer following strong-field ionization to tricationic states. Angle-resolved kinetic-energy correlation measurements reveal a direct Coulomb explosion pathway, as well as the delayed fragmentation mechanisms mediated by ultrafast intermolecular charge and proton transfer. In the indirect fragmentation paths, the kinetic energy distributions of the Cl^+ and HCl^+ fragments exhibit a pronounced angle-dependent splitting, evolving from a single peak to a double-peak structure as the relative emission angle $\theta_{Cl^+\text{-}HCl^+}$ approaches 180°. *Ab initio* calculations of the tricationic potential energy surface identify two competing dissociation pathways associated with charge-transfer and proton-transfer driven breakup processes, accounting for the observed spectral features. These results reveal how ultrafast charge redistribution and proton motion govern the strong-field dissociation dynamics of a prototypical hydrogen-bonded cluster.

Acknowledgements

This work was supported by the National Natural Science Foundation of China (Grants Nos. 12134005, 12450402, and 12450404) and the Fundamental Research Funds for the Central Universities.

References

[1] Ferray M, L'Huillier A, Li X F, Lompre L A, Mainfray G, and Manus C 1988 *J. Phys. B: At. Mol. Opt. Phys.* **21** L31
[2] Li M X, Tang X Y, Wang H Y, Li J L, Wang W T, Cai J A, Zhang J D, San X Y, Zhao X N, Ma P, Luo S Z, Jin C, and Ding D J 2025 *Light Sci. Appl.* **14** 181
[3] Isinger M, Squibb R J, Busto D, Zhong S, Harth A, Kroon D, Nandi S, Arnold C L, Miranda M, Dahlström J M, Lindroth E, Feifel R, Gisselbrecht M, and L'Huillier A 2017 *Science* **358** 893
[4] Jin W W, Jiang T, Liu J L, Luo S Z, Ren D X, Li X K, Wang C C, Lang Y, Wang X W, Zhao J, Zhao Z X, and Ding D J 2024 *Ultrafast Sci.* **4** 0066
[5] Li M X, Zhao L S, Wang H Y, Li J L, Wang W T, Cai J A, Hong X C, Shi X S, Zhang M, and Zhao X N 2025 *Sci. Adv.* **11** eadw5415
[6] Yuan H, Gao Y, Yang B, Gu S F, Lin H, Guo D L, Liu J L, Zhang S F, Ma X W, and Xu S Y 2024 *Phys. Rev. Lett.* **133** 193002
[7] Yu X T, Zhao X N, Wang Z Z, Yang Y Z, Zhang X Y, Ma P, Li X K, Wang C Y, Xu X P, and Wang C C 2021 *Phys. Rev. A* **104** 053104
[8] Yu X T, Zhang X Y, Hu X Q, Zhao X N, Ren D X, Li X K, Ma P, Wang C C, Wu Y, Luo S Z, and Ding D J 2022 *Phys. Rev. Lett.* **129** 023001
[9] Boll R, Schäfer J M, Richard B *et al.* 2022 *Nat. Phys.* **18** 423
[10] Li X K, Yu X T, Ma P, Zhao X N, Wang C C, Luo S Z, and Ding D J 2022 *Chin. Phys. B* **31** 103304
[11] Ma Q B, Hao X T, Zhou J Q, Xue X R, Zeng Q R, Li P, Wang L, and Ren X G 2025 *Chin. Phys. Lett.* **43** 010301
[12] Jin W W, Wang C C, Zhao X G, Yang Y Z, Ren D X, Liu Z J, Li X K, Luo S Z, and Ding D J 2024 *Chin. Phys. Lett.* **41** 053101
[13] Dantus M 2024 *Science* **385** eadk1833
[14] Wang S F and Wu C Y 2025 *Chin. J. Chem. Phys.* **38** 523
[15] Jahnke T, Sann H, Havermeier T *et al.* 2010 *Nat. Phys.* **6** 139

[16] Wei L, Lam C S, Zhang Y, Ren B H, Han J, Wang B, Zou Y M, Chen L, Lau K C, and Wei B R 2021 *J. Phys. Chem. Lett.* **12** 5789
[17] Dereka B, Yu Q, Lewis N H C, Carpenter W B, Bowman J M, and Tokmakoff A 2021 *Science* **371** 160
[18] Green A E, Chen K Y, Bhattacharyya S, Allum F, Usenko S, Ashfold M N R, Baumann T M, Borne K D, Brouard M, and Burt M 2025 *J. Am. Chem. Soc.* **147** 37133
[19] Zhou J Q, Wu L, Belina M, Skitnevskaya A D, Jia S K, Xue X R, Hao X T, Zeng Q R, Ma Q B, and Zhao Y T 2025 *Nat. Commun.* **16** 5838
[20] Wang E L, Ren X G, and Dorn A 2021 *Phys. Rev. Lett.* **126** 103402
[21] Zhou J Q, Hu X Q, Xue X R, Hao X T, Wang L, Li P, Ma Q B, He L H, Wang C C, and Wu Y 2026 *Fundam. Res.* (in press)
[22] Ren X G, Wang E L, Skitnevskaya A D, Trofimov A B, Gokhberg K, and Dorn A 2018 *Nat. Phys.* **14** 1062
[23] Mishra D, LaForge A C, Gorman L M, Díaz-Tendero S, Martín F, and Berrah N 2024 *Nat. Commun.* **15** 6656
[24] Loh Z H, Doumy G, Arnold C, Kjellsson L, Southworth S H, Al Haddad A, Kumagai Y, Tu M F, Ho P J, and March A M 2020 *Science* **367** 179
[25] Yang J, Dettori R, Nunes J P F, List N H, Biasin E, Centurion M, Chen Z J, Cordones A A, Deponte D P, and Heinz T F 2021 *Nature* **596** 531
[26] Ekanayake N, Severt T, Nairat M, Weingartz N P, Farris B M, Kaderiya B, Feizollah P, Jochim B, Ziaee F, and Borne K 2018 *Nat. Commun.* **9** 5186
[27] Ma P, Wang C C, Li X K, Yu X T, Tian X, Hu W H, Yu J Q, Luo S Z, and Ding D J 2017 *J. Chem. Phys.* **146** 244305
[28] Ekanayake N, Nairat M, Kaderiya B, Feizollah P, Jochim B, Severt T, Berry B, Pandiri K R, Carnes K D, and Pathak S 2017 *Sci. Rep.* **7** 4703
[29] Zhang Y, Ren B H, Yang C L, Wei L, Wang B, Han J, Yu W D, Qi Y Y, Zou Y M, and Chen L 2020 *Commun. Chem.* **3** 160
[30] Mi Y H, Wang E L, Dube Z, Wang T, Naumov A Y, Villeneuve D M, Corkum P B, and Staudte A 2023 *Nat. Chem.* **15** 1224
[31] Zhou L R, Ni H C, Jiang Z J, Qiang J J, Jiang W Y, Zhang W B, Lu P F, Wen J, Lin K, and Zhu M F 2023 *Nat. Chem.* **15** 1229
[32] Huang H, Hou H M, Wen J, Ni H C, and Wu J 2024 *Phys. Rev. A* **109** 043107
[33] Jiang Z J, Huang H, Lu C X, Zhou L R, Pan S Z, Qiang J J, Shi M H, Ye Z J, Lu P F, and Ni H C 2024 *Nat. Commun.* **15** 2854
[34] Low P J, Chu W B, Nie Z G, Bin Mohd Yusof M S, Prezhdo O V, and Loh Z H 2022 *Nat. Commun.* **13** 7300
[35] Thürmer S, Ončák M, Ottosson N, Seidel R, Hergenhahn U, Bradforth S E, Slavíček P, and Winter B 2013 *Nat. Chem.* **5** 590
[36] Zhong Q, Poth L, Ford J V, and Castleman Jr A W 1998 *Chem. Phys. Lett.* **286** 305
[37] Hoshina K, Hagihara H, and Tsuge M 2012 *J. Phys. Chem. A* **116** 826
[38] Zhou J Q, Belina M, Jia S K, Xue X R, Hao X T, Ren X G, and Slavíček P 2022 *J. Phys. Chem. Lett.* **13** 10603
[39] Zhou J Q, Jia S K, Hu X Q, Wang E L, Xue X R, Wu Y, Wang J G, Dorn A, and Ren X G 2023 *Phys. Rev. Lett.* **130** 233001
[40] Zhang X Y, Zhao X N, Liu H, Yin Z Y, Zhao X G, Ma P, Li X K, Wang C C, Wang Q X, and Luo S Z 2024 *Phys. Rev. A* **109** 023112
[41] Zhao X N, Zhang X Y, Liu H, Ma P, Li X K, Wang C C, Luo S Z, and Ding D J 2025 *Phys. Rev. A* **111** 053106
[42] Shi M H, Lu C X, Jiang Z J, Ye Z J, Chen J X, Long X L, Hu Y, Zhao W X, Zhang W B, and Wu J 2025 *Phys. Rev. A* **112** 043102
[43] Ren X G, Zhou J Q, Wang E L, Yang T, Xu Z F, Sisourat N, Pfeifer T, and Dorn A 2022 *Nat. Chem.* **14** 232
[44] Gao Y, Skitnevskaya A D, Wang E L, Yuan H, Ren X G, Lin H, Yan Z Y, Zhang S F, Gu S F, and Yang B 2025 *Phys. Rev. X* **15** 011053
[45] Pitzer M, Kunitski M, Johnson A S, Jahnke T, Sann H, Sturm F, Schmidt L P H, Schmidt-Böcking H, Dörner R, and Stohner J 2013 *Science* **341** 1096
[46] Endo T, Neville S P, Wanie V, Beaulieu S, Qu C, Deschamps J, Lassonde P, Schmidt B E, Fujise H, and Fushitani M 2020 *Science* **370** 1072
[47] Lam H V S, Venkatachalam A S, Bhattacharyya S, Chen K Y, Borne K, Wang E L, Boll R, Jahnke T, Kumarappan V, and Rudenko A 2024 *Phys. Rev. Lett.* **132** 123201
[48] Lam H V S, Hoang V H, Venkatachalam A S, Bhattacharyya S, Chen K Y, Jacob S, Kudagama S, Nguyen T T, Rolles D, and Thumm U 2025 *Phys. Rev. A* **111** L061101
[49] Richard B, Boll R, Banerjee S, Schäfer J M, Jurek Z, Kastirke G, Fehre K, Schöffler M S, Anders N, and Baumann T M 2025 *Science* **389** 650
[50] Dörner R, Mergel V, Jagutzki O, Spielberger L, Ullrich J, Moshammer R, and Schmidt-Böcking H 2000 *Phys. Rep.* **330** 95
[51] Ullrich J, Moshammer R, Dorn A, Dörner R, Schmidt L P H, and Schmidt-Böcking H 2003 *Rep. Prog. Phys.* **66** 1463
[52] Zhao X N, Xu T, Yu X T, Ren D X, Zhang X Y, Li X K, Ma P, Wang C C, Zhang D D, Wang Q X, Hu X Q, Luo S Z, Wu Y, Wang J G, and Ding D J 2021 *Phys. Rev. A* **103** 053103
[53] Zeller S, Kunitski M, Voigtsberger J, Waitz M, Trinter F, Eckart S, Kalinin A, Czasch A, Schmidt L P H, and Weber T 2018 *Phys. Rev. Lett.* **121** 083002
[54] Tao F M and Klemperer W 1995 *J. Chem. Phys.* **103** 950
[55] Qiu Y H and Bačič Z 1997 *J. Chem. Phys.* **106** 2158
[56] Knowles P J and Werner H J 1985 *Chem. Phys. Lett.* **115** 259
[57] Werner H J, Knowles P J, Knizia G, Manby F R, and Schütz M 2012 *WIREs Comput. Mol. Sci.* **2** 242
[58] Zhao X N, Yu X T, Xu X P, Yin Z Y, Yu J Q, Li X K, Ma P, Zhang D D, Wang C C, and Luo S Z 2020 *Phys. Rev. A* **101** 013416
[59] Ma J Y, Li H, Lin K, Song Q Y, Ji Q Y, Zhang W B, Li H X, Sun F H, Qiang J J, and Lu P F 2018 *Phys. Rev. A* **97** 063407
[60] Teixidor M M, Pirani F, Candori P, Falcinelli S, and Vecchiocattivi F 2003 *Chem. Phys. Lett.* **379** 139